Millijoule Femtosecond X-Ray Pulses from an Efficient Fresh-Slice Multistage Free-Electron Laser

Guanglei Wang, Philipp Dijkstal, Sven Reiche, Kirsten Schnorr, and Eduard Prat*
Paul Scherrer Institut, CH-5232 Villigen PSI, Switzerland

(Received 16 October 2023; accepted 18 December 2023; published 19 January 2024)

We present the generation of x-ray pulses with average pulse energies up to one millijoule and rms pulse durations down to the femtosecond level. We have produced these intense and short pulses by employing the fresh-slice multistage amplification scheme with a transversely tilted electron beam in a free-electron laser. In this scheme, a short pulse is produced in the first stage and later amplified by fresh parts of the electron bunch in up to a total of four stages of amplification. Our implementation is efficient, since practically the full electron beam contributes to produce the x-ray pulse. Our implementation is also compact, utilizing only 32 m of undulator. The demonstration was done at Athos, the soft x-ray beamline of SwissFEL, which was designed with high flexibility to take full advantage of the multistage amplification scheme. It opens the door for scientific opportunities following ultrafast dynamics using nonlinear x-ray spectroscopy techniques or avoiding electronic damage when capturing structures with a single intense pulse via single-particle imaging.

DOI: 10.1103/PhysRevLett.132.035002

X-ray free-electron lasers (FELs) are modern scientific instruments capable of studying matter with spatial and temporal resolutions at the scale of atomic processes [1–10]. The x-ray FEL radiation is produced by a high-brightness electron beam with GeV energies traveling through an undulator beamline. Standard x-ray FEL pulses have durations of few tens of femtoseconds and peak powers of tens of gigawatts, corresponding to pulse energies at the millijoule level.

Newly emerging experimental techniques, such as nonlinear x-ray spectroscopy [11–17], stimulated Raman scattering [18], or single-particle imaging [19–23], greatly benefit from higher-power and shorter x-ray pulses than in standard FEL configurations. These applications require the absorption of multiple x-ray photons each of which individually triggers an electronic relaxation cascade by creating a core or inner-valence hole, which decays within a few femtoseconds or faster, e.g., via Auger decay. Thus, within a standard FEL pulse duration of a few tens of femtoseconds, multiple photoionization-Auger cycles can occur, producing an increasingly charged and excited target over the course of the x-ray pulse [24]. For instance, single-particle imaging aims at taking a snapshot of a particle with one intense FEL pulse before the structure is destroyed. Thus, in order to outrun electronic damage [25], which is caused by multiple photoionization and decay cycles, pulses shorter than Auger lifetimes are required [26].

To first approximation, the FEL pulse duration is determined by the extent of the part of the electron pulse whose quality is sufficient to drive the FEL process. Femtosecond and subfemtosecond x-ray FEL pulses have been achieved either by strongly compressing the electron beam or by limiting the lasing part of the electron beam to a small region with spoiling schemes. See Refs. [27–33] for demonstration examples of x-ray FEL pulses with sub-femtosecond durations.

Methods based on fresh-slice multistage amplification following the so-called superradiance regime [34,35] have been proposed to increase the power of short FEL pulses [36–39]. These schemes are based on tailoring the electron beam in such a way that a fresh part of the electron beam can be provided at each amplification stage. Several approaches have been proposed to achieve this, based on current peaks in the electron distribution with external lasers [36,39], spoiling the electron beam emittance with multiple-slotted foils [37], or exploiting a transverse tilt of the electron beam [38]. The latter approach, proposed by some of the authors of this work, has important advantages: it is efficient, since potentially the full electron beam can contribute to the FEL pulse; the pulse duration can easily be tuned by adjusting the tilt amplitude [larger (smaller) tilts correspond to shorter (longer) pulses with less (more) energy]; and it is relatively simple, since, besides standard components of an FEL facility, from which the tilt can be generated, it only requires small magnetic chicanes between certain undulator modules. One disadvantage is that, since the transverse extension of the beam is large because of the tilted beam, there can be operational issues related to beam loss. Fresh-slice multistage amplification has so far only been demonstrated at the Linac Coherent Light Source applying the beam tilt method [40]: the authors reported the production of 670 eV pulses with

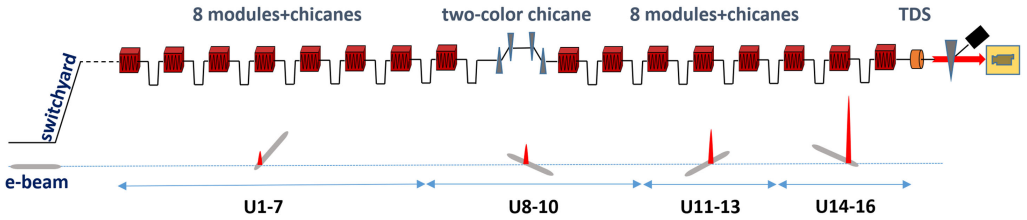

FIG. 1. Top: schematic layout of the Athos beamline (not to scale). The undulator beamline consists of 16 undulator modules interleaved with magnetic chicanes. In addition, there is a larger chicane in the middle of the beamline (two-color chicane). Bottom: illustration of the fresh-slice multistage scheme for four amplification stages. The electron beam (gray ellipse) is transversely tilted in the switchyard before the undulator beamline. The tilt orientation changes due to the focusing strength of the quadrupole magnets along the undulator. The beam tail produces a short FEL pulse (shown in red) in the first stage (undulators U1–U7), which is later amplified by other parts of the electron beam in the next stages (U8–10, U11–13, and U14–16). The longitudinal overlap between the FEL pulse and the electrons is achieved with the chicane delays, and the transverse overlap by trajectory correction. An x-band transverse deflecting structure (TDS) is used for time-resolved diagnostics of the electron and photon beams. See text for more details.

pulse energies of a few hundreds of microjoules and durations of a few femtoseconds using up to three amplification stages.

Here, we report the generation of x-ray pulses with unprecedented performance using the fresh-slice multistage amplification scheme with a transversely tilted beam. We demonstrate the efficient use of practically the entire electron beam with up to four amplification stages, resulting in the production of x-ray pulses with millijoule energies and estimated rms durations at the femtosecond level. We present time-resolved and gain curve measurements showing these results. This performance level is achieved with only 32 m of undulator length, which is possible thanks to the use of the optical klystron mechanism [41] in the first modules to reduce the required length of the first amplification stage. The demonstration was done at the soft x-ray beamline of SwissFEL called Athos [42], which has been in user operation since 2022 and whose design was optimized to fully exploit the fresh-slice multistage amplification method. In particular, Athos has a magnetic chicane between every two undulator modules, so that the number of amplification stages can be freely chosen to achieve the best performance in a given case.

Figure 1 shows a sketch of Athos along with an illustration of the method. Athos covers the photon energy range between 0.26 and 1.9 keV. SwissFEL usually operates with electron beams with charges of 200 pC and electron pulse durations between 15 and 30 fs (rms). The electron beam energy at Athos is normally around 3.4 GeV, but can be tuned down to 2.9 GeV. The undulator beamline consists of 16 APPLE-X modules [43] of 2 m total length each, featuring 38 mm period and capable of providing variable field and polarization. There is a small magnetic chicane (0.2 m length) between every two undulator modules. The chicanes consist of four dipole magnets and are fundamental for the work demonstrated here. Each chicane can delay the electron beam by up to about 7 fs and produce a transverse offset up to a few hundreds of micrometers. The space between two undulator modules measures 0.8 m and it hosts, besides the chicanes, a quadrupole magnet, a dipole corrector magnet, and a beam-position monitor used to control the electron beam trajectory. A larger chicane, primarily used for two-color operation [44], is installed in the middle of the undulator beamline. After the undulator beamline an x-band radio frequency transverse deflecting structure (TDS) enables measurements of the time-resolved properties of the electron beam with a resolution below one femtosecond [45]. A scintillator screen placed at the Athos beam dump after the undulator allows, in combination with the TDS, the longitudinal phase space (LPS, energy vs time) of the electron beam to be measured. Comparing the LPS between lasing-on and lasing-off conditions we can reconstruct the FEL power profile [46,47]. A gas detector after the undulator beamline measures the pulse energy of the FEL radiation [48]. Moreover, a photon spectrometer [49] is available to measure the FEL spectra.

The bottom of Fig. 1 shows a sketch of the method. In our implementation, the electron beam is transversely tilted before the undulator beamline. To this end we leak out dispersion in the Athos switchyard by changing the field of a quadrupole magnet in a dispersive location. This, combined with the fact that the beam has a residual energy chirp from the bunch compression at the location of the quadrupole magnet, results in a transversely tilted beam [50]. Specifically in our case, the dispersion value at the quadrupole magnet is around 0.2 m, the energy chirp is around 0.5% (rms), and we change the quadrupole magnet strength by about 10%–20% (the initial integrated normalized gradient along the quadrupole is 0.264 m^{-1}). This results in dispersion values at the undulator of up to 10 cm, which correspond to tilted beams with transverse beam sizes of up to about 0.5 mm (rms). This type of dispersion-based streaking is simple, uses standard components of the facility, and produces linear beam tilts as long as the energy chirp is linear. In our case, the transverse tilt could also be achieved by employing the wakefields of corrugated structures, as it was done in Ref. [40], which are

installed in Athos before the undulator (not shown in Fig. 1). This approach has, however, the disadvantage of producing a nonlinear tilt, which makes it difficult to utilize the full electron bunch in the fresh-slice multistage amplification approach. Moreover, the dispersion-based tilt is more robust against trajectory jitter of the electron beam. Finally, in our case, dispersion-based streaking entails lower beam losses than the wakefield method.

Once the beam is transversely tilted, we align the tail of the bunch in the first undulator section using standard trajectory correction methods. The tail produces a short FEL pulse in the first undulator section until the FEL process has reached saturation, while the other parts of the electron beam are misaligned and therefore do not contribute to lasing. We use the optical klystron effect [41] in the first undulator stage to reduce the required undulator length to reach FEL saturation by about 20%–25%, such that more modules are available in subsequent stages. For this, we optimize the longitudinal dispersion of the first three to four chicanes (the longitudinal dispersion is about twice the delay), with corresponding delay values of about 1 fs or less in each chicane. The short FEL pulse produced in the first stage is later amplified by the other parts of the electron beam in the next stages. To achieve that, we need to overlap the FEL pulse with the fresh electrons, both temporally and transversely, before the beginning of each amplification stage. The temporal overlap is achieved with the chicanes between the modules. For the transverse overlap, we use the offset produced by the chicanes and the corrector magnets in the undulator to align the fresh part of the electron beam in the undulator. We taper the undulator field of the last two modules of the first stage to maximize the extracted FEL power. Moreover, we also optimize the undulator field of the modules of the next stages for maximum pulse energy.

Figure 2 shows the results obtained for a photon energy of 520 eV. The total duration of the electron beam was around 10 fs (rms), the current profile was rather flat except at the bunch head and tail, the bunch charge was 200 pC, and the beam energy was 3.4 GeV. The number of amplification stages was chosen to maximize the output power. We worked with four stages of amplification: the first stage with seven undulator modules, the rest with three undulator modules each. The delays between the amplification stages were set to 5 fs each. To maximize the pulse energy, we worked with a tilt amplitude for which virtually the entire bunch contributed to lasing after four stages, corresponding to an approximate FEL pulse duration equal to the total electron beam duration divided by the number of stages. If shorter pulses are needed, the tilt can be increased and smaller delays can be used, which would allow for more stages (requiring a longer undulator) or allow operating with shorter electron bunches.

Figure 2(a) displays single-shot LPS measurements without lasing (top plot) and after each amplification stage (subsequent plots). The beam was horizontally streaked, thus adding up the TDS tilt and the dispersion-based tilt used to create the short pulses. The time calibration, i.e., the parameter converting the transverse coordinate in the streaking direction to the time coordinate along the bunch, is calculated to be 92 μm/fs based on the implemented delays and the FEL slippage between the different amplification stages (see Supplemental Material [51]). The energy axis of the LPS is obtained by scaling the vertical coordinates with the vertical dispersion value of 19.4 cm defined by the dipole and quadrupole magnets before the screen.

The effect of the FEL process, i.e., an energy loss and an energy spread increase, is clearly seen in Fig. 2(a). In the first stage only the tail (right-hand part) of the bunch is lasing, in the next stages the other parts of the electron beam are subsequently contributing to the FEL process. At the end, most of the electron beam has contributed to enhance one short FEL pulse. Figure 2(b) shows the FEL gain curve measured with the gas detector. In the first stage, the FEL process reaches saturation. The FEL pulse energy is further increased well beyond saturation in the subsequent stages with different parts of the bunch, a likely indication of the FEL superradiance regime. To unequivocally prove superradiance, an increase of the peak power with the square of the undulator length and a reduction of the spike FEL duration with the square root of the undulator length would have to be demonstrated, something that was not possible with our setup. The final average pulse energy is 1.05 mJ.

Figures 2(c) and 2(d) display reconstructed FEL power profiles for 20 consecutive shots. The profiles are derived from the time-resolved energy loss and energy spread increase between the different amplification stages (see Supplemental Material [51]). The energy loss method provides an absolute measurement of the FEL profiles, while the relative results from the energy spread approach are calibrated with the pulse energies measured with the gas detector. The nature of the multistage amplification process precludes a rigorously accurate shot-to-shot reconstruction of the FEL power profile based on electron energy loss and energy spread increase. In order to still arrive at estimates for peak power and pulse durations, we apply two approximate methods for reconstructing FEL power profiles. In the first, shown in Fig. 2(c), we construct FEL power profiles by comparing the shot-to-shot time-resolved energy properties of the final stage and the average properties of the previous amplification stage, assuming that all pulse energy goes to this final FEL power profile. This is rather well justified considering that there is a clean and consistent amplification between the different stages. Nevertheless, this method may overestimate the real performance, since only in an ideal case all the FEL pulse in a certain stage will be amplified in the following stage. In particular, the FEL power profile from the first stage is somewhat longer than

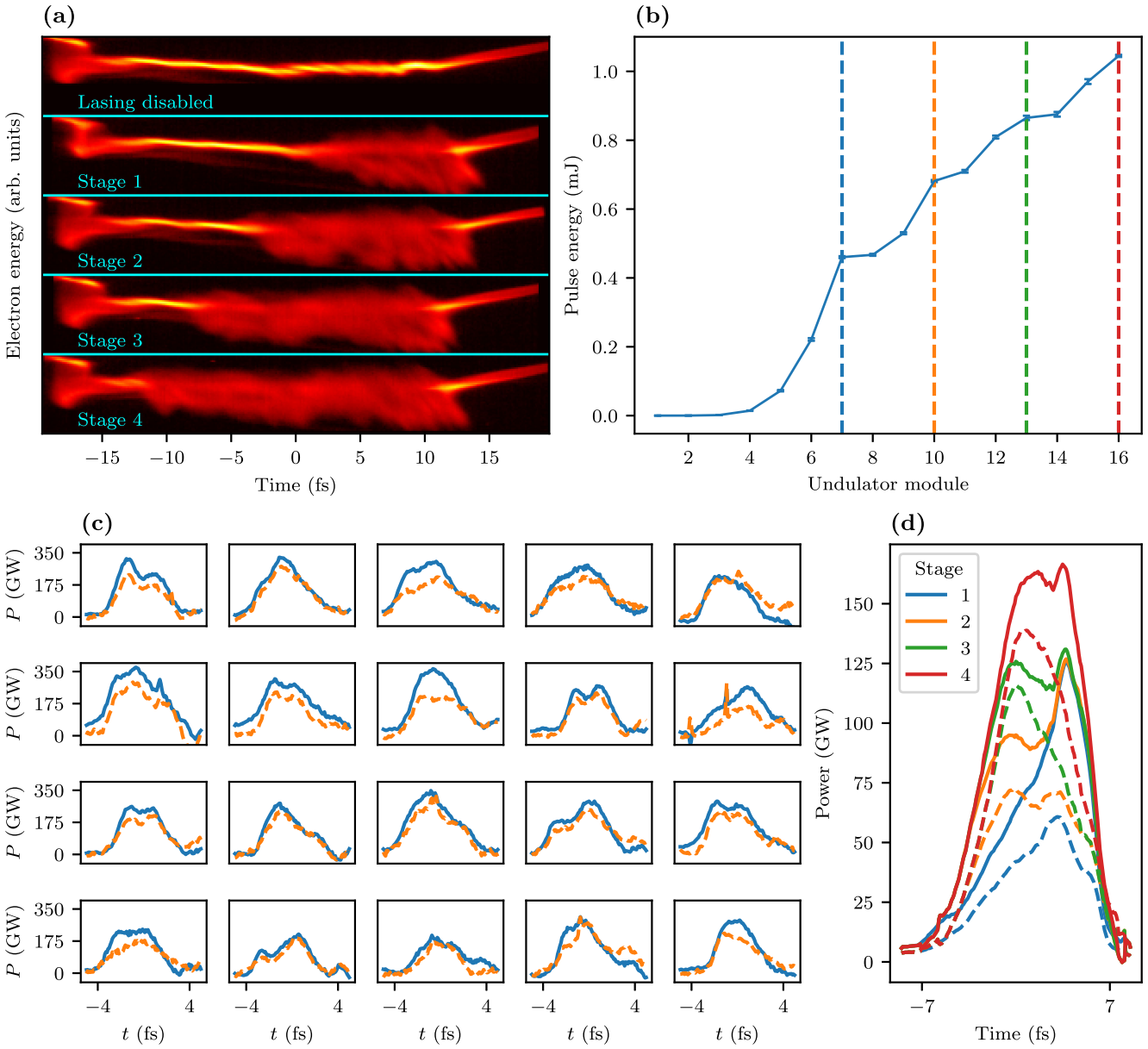

FIG. 2. Results for a photon energy of 520 eV. (a) Single-shot LPS measurements without lasing and after each amplification stage. The head of the bunch is on the left. (b) FEL gain curve. The dashed lines delimit the four stages of amplification. (c) Reconstructed shot-to-shot FEL power profiles at the undulator exit for 20 consecutive shots. (d) Reconstructed average power profiles after each amplification stage. In (c) and (d) the solid lines show results obtained from the energy loss of the electron beam, the dashed lines from the energy spread increase.

the ones from the next stages. On the other hand, the true FEL performance may also be underestimated due to resolution and slippage effects.

In this way we reconstruct average peak powers of around 250 GW and average rms pulse durations of around 1.9 fs. More precisely, the energy loss method gives an average peak power of 289 ± 46 GW and an average pulse duration of 1.87 ± 0.22 fs over the 20 shots, while we obtain 240 ± 39 GW and 1.93 ± 0.22 fs from the energy spread increase of the electron beam. The quoted errors reflect standard deviations over the 20 shots, i.e., are statistical only. The maximum peak power measured among the 20 shots (applying the energy loss method) is 374 GW, the minimum pulse duration 1.32 fs (not from the same shot).

In the second reconstruction method, we settle for average values. Figure 2(d) shows the average FEL power profiles after each amplification stage from the electron beam properties averaged over the same 20 shots. Average FEL power profiles from each stage are stacked, after being shifted in time by the known time delay introduced by the chicanes and slippage effects. The final average peak

powers and rms pulse durations are 167 GW and 3.03 fs from the energy loss approach, and 139 GW and 2.95 fs from the energy spread method. These quantities underestimate the real performance since shot-to-shot time jitter will result in an artificial increase of the pulse duration and decrease of the peak power as calculated here. In general, we observe rather good agreement between the two approaches to reconstruct the FEL power profile (from the energy loss and from the energy spread increase of the electron beam). Nevertheless, the energy spread approach gives lower peak powers than the energy loss method, especially for the average profiles. This discrepancy could arise from the two independent ways to obtain the FEL pulse energy in the two methods (direct energy loss and calibration with gas detector for the energy spread approach). In fact, the reconstructed pulse energy from the energy loss approach (i.e., the integral of the average power profile) is 1.38 mJ, significantly higher than the 1.05 mJ given by the gas detector. All in all, we can claim with some certainty that we have generated FEL pulses with peak powers of around 200 GW and durations of a few femtoseconds. Spectral measurements presented in the Supplemental Material are consistent with having pulses of a few femtoseconds or shorter [51].

We have obtained similar results in other shifts and for different photon energies. In particular, for a photon energy of 1 keV, we measured a pulse energy of 0.84 mJ and reconstructed shot-to-shot peak powers of around 200 GW along with rms pulse durations of around 1.5 fs. In this case, we used a setup with three amplification stages. The first stage consisted of eight modules, the second and third of four modules each. This is consistent with the fact that the FEL process requires more undulator length to achieve saturation at shorter wavelengths. The two delays between the amplification stages were set to 10 and 5 fs. We used one small chicane and the two-color chicane to set the 10 fs delay. In this case, the reconstructed pulse energy from the energy loss approach is 0.85 mJ, fitting very well with the value measured by the gas detector (0.84 mJ).

To conclude, we have generated x-ray pulses with millijoule energies and femtosecond durations at Athos using the fresh-slice multistage amplification scheme with a tilted beam. We emphasize that our implementation is both efficient, making use of essentially the entire electron bunch in the FEL process, and compact, requiring only 32 m of undulators, thanks to the exploitation of the optical klystron effect in the first amplification stage. The performance of the scheme in terms of peak power and pulse duration is limited by the available active undulator length of only 32 m (16 modules of 2 m each) and by the beam tilt amplitude, which cannot be increased further without generating beam losses incompatible with safe operation. The latter limitation arises from the effective vacuum aperture of our undulator beamline of only about 3 mm. We expect that the implementation of this scheme in other x-ray FEL facilities with longer undulators and lower sensitivity to beam losses could produce x-ray pulses with peak powers of more than one terawatt and durations well below half a femtosecond. The fresh-slice multistage amplification scheme using an electron beam with unevenly separated current peaks, as proposed in Ref. [39], would be another possibility to achieve shorter pulses, in principle associated to less losses. Our work paves the way for new discoveries in FEL applications requiring high-power and short FEL pulses such as single-particle imaging or nonlinear spectroscopy.

We acknowledge Thomas Schietinger for improving the language and consistency of the manuscript. We thank all the technical groups involved in the operation of SwissFEL for support.

*eduard.prat@psi.ch

[1] B. W. J. McNeil and N. R. Thompson, Nat. Photonics **4**, 814 (2010).
[2] C. Pellegrini, A. Marinelli, and S. Reiche, Rev. Mod. Phys. **88**, 015006 (2016).
[3] C. Bostedt, S. Boutet, D. M. Fritz, Z. Huang, H. J. Lee, H. T. Lemke, A. Robert, W. F. Schlotter, J. J. Turner, and G. J. Williams, Rev. Mod. Phys. **88**, 015007 (2016).
[4] W. Ackermann, G. Asova, V. Ayvazyan, A. Azima, N. Baboi, J. Bähr, V. Balandin, B. Beutner, A. Brandt, A. Bolzmann *et al.*, Nat. Photonics **1**, 336 (2007).
[5] P. Emma, R. Akre, J. Arthur, R. Bionta, C. Bostedt, J. Bozek, A. Brachmann, P. Bucksbaum, R. Coffee, F.-J. Decker *et al.*, Nat. Photonics **4**, 641 (2010).
[6] T. Ishikawa, H. Aoyagi, T. Asaka, Y. Asano, N. Azumi, T. Bizen, H. Ego, K. Fukami, T. Fukui, Y. Furukawa *et al.*, Nat. Photonics **6**, 540 (2012).
[7] E. Allaria, D. Castronovo, P. Cinquegrana, P. Craievich, M. D. Forno, M. B. Danailov, G. D'Auria, A. Demidovich, G. D. Ninno, S. D. Mitri *et al.*, Nat. Photonics **7**, 913 (2013).
[8] H.-S. Kang, C.-K. Min, H. Heo, C. Kim, H. Yang, G. Kim, I. Nam, S. Y. Baek, H.-J. Choi, G. Mun *et al.*, Nat. Photonics **11**, 708 (2017).
[9] W. Decking, S. Abeghyan, P. Abramian, A. Abramsky, A. Aguirre, C. Albrecht, P. Alou, M. Altarelli, P. Altmann, K. Amyan *et al.*, Nat. Photonics **14**, 391 (2020).
[10] E. Prat, R. Abela, M. Aiba, A. Alarcon, J. Alex, Y. Arbelo, C. Arrell, V. Arsov, C. Bacellar, C. Beard *et al.*, Nat. Photonics **14**, 748 (2020).
[11] S. Tanaka and S. Mukamel, Phys. Rev. Lett. **89**, 043001 (2002).
[12] S. Mukamel, D. Healion, Y. Zhang, and J. D. Biggs, Annu. Rev. Phys. Chem. **64**, 101 (2013).
[13] C. Weninger, M. Purvis, D. Ryan, R. A. London, J. D. Bozek, C. Bostedt, A. Graf, G. Brown, J. J. Rocca, and N. Rohringer, Phys. Rev. Lett. **111**, 233902 (2013).
[14] F. Bencivenga, R. Cucini, F. Capotondi, A. Battistoni, R. Mincigrucci, E. Giangrisostomi, A. Gessini, M. Manfredda, I. P. Nikolov, E. Pedersoli *et al.*, Nature (London) **520**, 205 (2015).

[15] T. Kroll, C. Weninger, R. Alonso-Mori, D. Sokaras, D. Zhu, L. Mercadier, V. P. Majety, A. Marinelli, A. Lutman, M. W. Guetg *et al.*, Phys. Rev. Lett. **120**, 133203 (2018).
[16] M. Fuchs, M. Trigo, J. Chen, S. Ghimire, S. Shwartz, M. Kozina, M. Jiang, T. Henighan, C. Bray, G. Ndabashimiye *et al.*, Nat. Phys. **11**, 964 (2015).
[17] Y. Zhang, T. Kroll, C. Weninger, Y. Michine, F. D. Fuller, D. Zhu, R. Alonso-Mori, D. Sokaras, A. A. Lutman, A. Halavanau *et al.*, Proc. Natl. Acad. Sci. U.S.A. **119**, e2119616119 (2022).
[18] V. Kimberg, A. Sanchez-Gonzalez, L. Mercadier, C. Weninger, A. Lutman, D. Ratner, R. Coffee, M. Bucher, M. Mucke, M. Agåker *et al.*, Faraday Discuss. **194**, 305 (2016).
[19] R. Neutze, R. Wouts, D. van der Spoel, E. Weckert, and J. Hajdu, Nature (London) **406**, 752 (2000).
[20] A. Aquila, A. Barty, C. Bostedt, S. Boutet, G. Carini, D. dePonte, P. Drell, S. Doniach, K. H. Downing, T. Earnest *et al.*, Struct. Dyn. **2**, 041701 (2015).
[21] M. M. Seibert, T. Ekeberg, F. R. N. C. Maia, M. Svenda, J. Andreasson, O. Jönsson, D. Odić, B. Iwan, A. Rocker, D. Westphal *et al.*, Nature (London) **470**, 78 (2011).
[22] T. Gorkhover, M. Adolph, D. Rupp, S. Schorb, S. W. Epp, B. Erk, L. Foucar, R. Hartmann, N. Kimmel, K.-U. Kühnel *et al.*, Phys. Rev. Lett. **108**, 245005 (2012).
[23] L. F. Gomez, K. R. Ferguson, J. P. Cryan, C. Bacellar, R. M. P. Tanyag, C. Jones, S. Schorb, D. Anielski, A. Belkacem, C. Bernando *et al.*, Science **345**, 906 (2014).
[24] L. Young, E. P. Kanter, B. Krässig, Y. Li, A. M. March, S. T. Pratt, R. Santra, S. H. Southworth, N. Rohringer, L. F. DiMauro *et al.*, Nature (London) **466**, 56 (2010).
[25] U. Lorenz, N. M. Kabachnik, E. Weckert, and I. A. Vartanyants, Phys. Rev. E **86**, 051911 (2012).
[26] P. J. Ho, B. J. Daurer, M. F. Hantke, J. Bielecki, A. A. Haddad, M. Bucher, G. Doumy, K. R. Ferguson, L. Flückiger, T. Gorkhover *et al.*, Nat. Commun. **11**, 167 (2020).
[27] S. Huang, Y. Ding, Y. Feng, E. Hemsing, Z. Huang, J. Krzywinski, A. A. Lutman, A. Marinelli, T. J. Maxwell, and D. Zhu, Phys. Rev. Lett. **119**, 154801 (2017).
[28] A. Marinelli, J. P. MacArthur, P. Emma, M. W. Guetg, C. Field, D. Kharakh, A. A. Lutman, Y. Ding, and Z. Huang, Appl. Phys. Lett. **111**, 151101 (2017).
[29] A. Malyzhenkov, Y. P. Arbelo, P. Craievich, P. Dijkstal, E. Ferrari, S. Reiche, T. Schietinger, P. Juranić, and E. Prat, Phys. Rev. Res. **2**, 042018(R) (2020).
[30] Z. Zhang, J. Duris, J. P. MacArthur, A. Zholents, Z. Huang, and A. Marinelli, New J. Phys. **22**, 083030 (2020).
[31] J. P. Duris, J. P. MacArthur, J. M. Glownia, S. Li, S. Vetter, A. Miahnahri, R. Coffee, P. Hering, A. Fry, M. E. Welch *et al.*, Phys. Rev. Lett. **126**, 104802 (2021).
[32] P. Dijkstal, Ph.D. thesis, ETH Zurich, 2022.
[33] E. Prat, A. Malyzhenkov, C. Arrell, P. Craievich, S. Reiche, T. Schietinger, and G. Wang, APL Photonics **8**, 111302 (2023).
[34] R. Bonifacio, L. D. S. Souza, P. Pierini, and N. Piovella, Nucl. Instrum. Methods Phys. Res., Sect. A **296**, 358 (1990).
[35] R. Bonifacio, N. Piovella, and B. W. J. McNeil, Phys. Rev. A **44**, R3441 (1991).
[36] T. Tanaka, Phys. Rev. Lett. **110**, 084801 (2013).
[37] E. Prat and S. Reiche, Phys. Rev. Lett. **114**, 244801 (2015).
[38] E. Prat, F. Löhl, and S. Reiche, Phys. Rev. ST Accel. Beams **18**, 100701 (2015).
[39] T. Tanaka, Y. W. Parc, Y. Kida, R. Kinjo, C. H. Shim, I. S. Ko, B. Kim, D. E. Kim, and E. Prat, J. Synchrotron Radiat. **23**, 1273 (2016).
[40] A. A. Lutman, M. W. Guetg, T. J. Maxwell, J. P. MacArthur, Y. Ding, C. Emma, J. Krzywinski, A. Marinelli, and Z. Huang, Phys. Rev. Lett. **120**, 264801 (2018).
[41] E. Prat, E. Ferrari, M. Calvi, R. Ganter, S. Reiche, and T. Schmidt, Appl. Phys. Lett. **119**, 151102 (2021).
[42] E. Prat, A. A. Haddad, C. Arrell, S. Augustin, M. Boll, C. Bostedt, M. Calvi, A. L. Cavalieri, P. Craievich, A. Dax *et al.*, Nat. Commun. **14**, 5069 (2023).
[43] T. Schmidt and M. Calvi, Synchrotron Radiat. News **31**, 35 (2018).
[44] E. Prat, P. Dijkstal, E. Ferrari, R. Ganter, P. Juranić, A. Malyzhenkov, S. Reiche, T. Schietinger, G. Wang, A. A. Haddad *et al.*, Phys. Rev. Res. **4**, L022025 (2022).
[45] P. Craievich, Z. Geng, F. Marcellini, C. Kittel, S. Reiche, T. Schietinger, G. Wang, and E. Prat, in *X-Ray Free-Electron Lasers: Advances in Source Development and Instrumentation VI*, edited by T. Tschentscher, L. Patthey, M. Zangrando, and K. Tiedtke, SPIE Proceedings Vol. 12581 (SPIE-International Society for Optical Engineering, Bellingham, WA, 2023).
[46] Y. Ding, C. Behrens, P. Emma, J. Frisch, Z. Huang, H. Loos, P. Krejcik, and M.-H. Wang, Phys. Rev. ST Accel. Beams **14**, 120701 (2011).
[47] C. Behrens, F.-J. Decker, Y. Ding, V. A. Dolgashev, J. Frisch, Z. Huang, P. Krejcik, H. Loos, A. Lutman, T. J. Maxwell *et al.*, Nat. Commun. **5**, 3762 (2014).
[48] A. A. Sorokin, Y. Bican, S. Bonfigt, M. Brachmanski, M. Braune, U. F. Jastrow, A. Gottwald, H. Kaser, M. Richter, and K. Tiedtke, J. Synchrotron Radiat. **26**, 1092 (2019).
[49] C. Arrell, V. Thominet, Y. Arbelo, U. Wagner, N. Gradwohl, E. Prat, L. Patthey, and R. Follath, in *Proceedings of the Conference on Lasers and Electro-Optics* (Optica Publishing Group, Washington, 2022).
[50] E. Prat and M. Aiba, Phys. Rev. ST Accel. Beams **17**, 032801 (2014).
[51] See Supplemental Material at http://link.aps.org/supplemental/10.1103/PhysRevLett.132.035002 for detailed information on the reconstruction algorithm of the FEL power profiles, including the determination of the time calibration, and FEL spectral measurements.